Received: 3 October 2019 | Revised: 25 February 2020 | Accepted: 26 March 2020

DOI: 10.1002/pld3.216

ORIGINAL RESEARCH

BdGT43B2 functions in xylan biosynthesis and is essential for seedling survival in *Brachypodium distachyon*

Deborah L. Petrik[1,2] | **Theodora Tryfona**[3] | **Paul Dupree**[3] | **Charles T. Anderson**[1]

[1]Department of Biology, The Pennsylvania State University, University Park, PA, USA

[2]Molecular Biology, Northeastern State University, Tahlequah, Oklahoma

[3]Department of Biochemistry, University of Cambridge, Cambridge, UK

Correspondence
Charles T. Anderson, Department of Biology, The Pennsylvania State University, University Park, PA, USA.
Email: cta3@psu.edu

Funding information
U.S. Department of Energy; Office of Science; Basic Energy Sciences

Abstract

Xylan is the predominant hemicellulose in the primary cell walls of grasses, but its synthesis and interactions with other wall polysaccharides are complex and incompletely understood. To probe xylan biosynthesis, we generated CRISPR/Cas9 knockout and amiRNA knockdown lines of *BdGT43B2*, an ortholog of the wheat *TaGT43-4* xylan synthase scaffolding protein in the *IRX14* clade, in *Brachypodium distachyon*. Knockout of *BdGT43B2* caused stunting and premature death in *Brachypodium* seedlings. Immunofluorescence labeling of xylans was greatly reduced in homozygous knockout *BdGT43B2* mutants, whereas cellulose labeling was unchanged or slightly increased. Biochemical analysis showed reductions in digestible xylan in knockout mutant walls, and cell size was smaller in knockout leaves. *BdGT43B2* knockdown plants appeared morphologically normal as adults, but showed slight reductions in seedling growth and small decreases in xylose content in isolated cell walls. Immunofluorescence labeling of xylan and cellulose staining was both reduced in *BdGT43B2* knockdown plants. Together, these data indicate that *BdGT43B2* functions in the synthesis of a form of xylan that is required for seedling growth and survival in *Brachypodium distachyon*.

KEYWORDS

artificial microRNA (amiRNA), *Brachypodium distachyon*, CRISPR/Cas9, glycosyl transferase, polysaccharide analysis by carbohydrate electrophoresis, xylan

1 | INTRODUCTION

The cell walls of eudicots and monocot grasses serve similar functions, two of which are to serve as a mechanical barrier to pests and pathogens, and to provide rigidity to permit vertical growth without structural collapse. Despite their common functions, compositional and structural differences exist between the cell walls of eudicots such as *Arabidopsis thaliana* (Arabidopsis) and monocot grass species such as *Brachypodium distachyon*. The type I primary cell walls (PCWs) of eudicots, non-commelinoid monocots, and gymnosperms share the presence of cellulose microfibrils embedded in a polysaccharide matrix in common with the type II primary cell walls of commelinoid monocots, which include grasses and sedges. However, the relative proportions of xyloglucan, xylan, pectins, and structural proteins differ significantly between type I and type II PCWs (Vogel, 2008), whereas type I PCWs contain xyloglucan as

the most prevalent hemicellulosic polysaccharide, type II PCWs contain glucuronoarabinoxylan (GAX) as the predominant hemicellulose and contain less pectin than type I PCWs. Eudicot species produce xylan in their secondary cell walls, but its composition differs from the GAX produced in the PCWs of grasses. In both cases, the xylan backbone is composed of β-1,4-linked xylose residues. However, the types and patterns of side group substitutions differ; eudicot xylan is typically only decorated with methylated or non-methylated glucuronic acids and acetyl groups, with rhamnose and galacturonic acid being found only at the reducing end of the xylan chain, whereas grass xylan is decorated with glucuronosyl and arabinosyl residues (Faik 2010). The arabinosyl residues may carry further substitutions (Wende & Fry 1997). Acetylated forms of the xylosyl sugars in the GAX backbone and the side decorations exist, resulting in GAX being more highly substituted than eudicot xylan (Rennie & Scheller 2014). The degree of xylan substitution affects its solubility, with solubility increasing as the number of substituted xylosyl residues increases (Köhnke, Östlund, & Brelid, 2011). The varying interactions of xylans with cellulose microfibrils, depending on their patterns of substitution, have been a recent area of study. In the secondary walls of *Arabidopsis thaliana*, an even pattern of xylan acetylation causes an even patterning of glucuronosylation, allowing xylan to fold into a twofold helical screw conformation in association with the hydrophilic face of cellulose (Busse-Wicher et al., 2014; Grantham et al., 2017; Simmons et al., 2016). In contrast, the more highly substituted GAX that exists in the PCWs of grasses might behave analogously to pectins, interacting with cellulose via mechanisms that are currently unclear and/or existing as soluble chains that are not associated with cellulose or other matrix polymers (Cosgrove, 2018).

Due to its variously substituted structure, xylan biosynthesis requires a suite of nucleotide sugar synthase, nucleotide sugar transporter, and transferase proteins (Rennie & Scheller, 2014). The glycosyltransferase family 43 (GT43) proteins IRREGULAR XYLEM (IRX) 9 and IRX14 were initially identified in Arabidopsis as contributing to xylan xylosyltransferase activity during secondary wall formation (Brown et al., 2007; Lee, O'Neill, Tsumuraya, Darvill, & Ye, 2007). Studies in Arabidopsis suggest that IRX9 and IRX14-related GT43s are both required for xylan synthesis, since IRX9 cannot complement *irx14* mutants and vice versa (Lee, Teng, Huang, Zhong, & Ye, 2010; Wu et al., 2010). Reduced expression of IRX10-related glycosyltransferases in family GT47 also led to reduced xylan synthesis activity in Arabidopsis (Brown, Zhang, Stephens, Dupree, & Turner, 2009) and rice (Chen, 2013), and IRX10-related proteins exhibit xylosyl transferase activity in vitro (Urbanowicz, Peña, Moniz, Moremen, & York 2014; Jensen, Johnson, & Wilkerson 2014).

The biochemical functions of the different GT proteins involved in xylan synthesis in vivo remain unclear, but it seems that GT43 proteins might be required for the activity of GT47 xylosyl transferases, perhaps by forming a protein complex (Zeng et al., 2016). Heterologous expression of the rice (*Oryza sativa*) ortholog of AtIRX9, OsIRX9, caused increased xylan synthase activity in Arabidopsis (Chiniquy et al, 2013), but this gene's inactivation in rice led to only modest reductions in xylan content and minor stunting (Chen et al, 2013), suggesting that other enzyme(s) such as IRX9-L or OsIRX14 might also contribute to xylan biosynthesis. In wheat (*Triticum aestivum*), RNAi of orthologues of IRX9 or IRX10 in the endosperm reduced xylan biosynthesis (Freeman et al., 2016). Proper trafficking of a six-member xylan synthase complex (XSC) to the Golgi and maximal xylan synthase activity only occurred if wheat IRX10 (TaGT47-13), and IRX14 (TaGT43-4) were both present and functional (Jiang et al., 2016). Fusions of wheat XSC components with fluorescent reporters indicated that TaGT43-4 serves as a structural scaffold for the complex, permitting its complete assembly and transport from the ER to the Golgi apparatus (Jiang et al., 2016). In Arabidopsis, a point mutation in the predicted catalytic amino acid of IRX14 was able to rescue the *irx14* mutant phenotype, suggesting that IRX14 has mostly a structural role (Ren, Hansen, Ebert, Lau, & Scheller, 2014). However, it cannot be ruled out that IRX14 may also have limited catalytic activity, as the ability of IRX14 to bind to the xylosyl substrate was found to be critical to complementing the *irx14* mutant (Ren et al., 2014).

TaIRX14 was shown to be a component of a protein complex derived from purified wheat microsomes derived from etiolated wheat seedlings. This protein purification derived from wheat etiolated seedling microsomes exhibited xylosyltransferase activity (Zeng Chatterjee, & Faik 2008; Zeng et al., 2010). Rice *OsIRX9*, *OsIRX9L*, and *OsIRX14* genes were overexpressed in Arabidopsis *irx9* and *irx14* mutants to demonstrate complementation, providing evidence that *OsIRX9*, *OsIRX9L*, and *OsIRX14* were orthologs to the Arabidopsis *IRX9* and *IRX14* genes, respectively (Chiniquy et al, 2013). RNAi of *IRX10 TaGT47_2* and *IRX9 TaGT43_2* was shown to reduce xylan biosynthesis in wheat starchy endosperm cells, through the use of a tissue-specific promoter (Lovegrove et al., 2013). However, growth and development phenotypes in vegetative tissues were not reported. Finally, TaGT43_2 was shown to be necessary for xylan synthesis in endosperm by examining wheat flour produced by TaGT43_2 RNAi versus wild-type wheat. This publication reported using the same method to create the TaGT43_2 RNAi plants as Ref. (Lovegrove et al., 2013), which would presumably include the use of the starchy endosperm-specific promoter to drive TaGT43_2 RNAi. T-DNA insertion derived double knockout of *IRX14* and *IRX14L* in Arabidopsis was shown to be associated with severely stunted plants that failed to produce an inflorescence (Keppler & Showalter, 2010). Interestingly, these plants were reported to grow normally for the first week, but then cease growth. Further, premature death was not reported as a phenotype. Thus, to our knowledge, no published report of growth and developmental phenotypes resulting from IRX14 knockdown or knockout exists that is specific to grasses, which is relevant because of their unique cell wall composition in comparison to dicots.

Brachypodium distacyhon is a useful model species for the analysis of grass cell walls because it is diploid, has a small stature and an 8–10 week seed-to-seed life cycle, has a sequenced genome, and is relatively easy to transform (Vogel et al., 2010). The composition of its cell walls has been characterized (Rancour, Marita, & Hatfield, 2012). Phylogenetic analysis of *Brachypodium distachyon* GT43 members shows that there are eight members in Clade A and two members in Clade B (Whitehead et al., 2018). RNAi knockdown of one these *GT43* genes, *Bradi5g24290*, results in modestly reduced

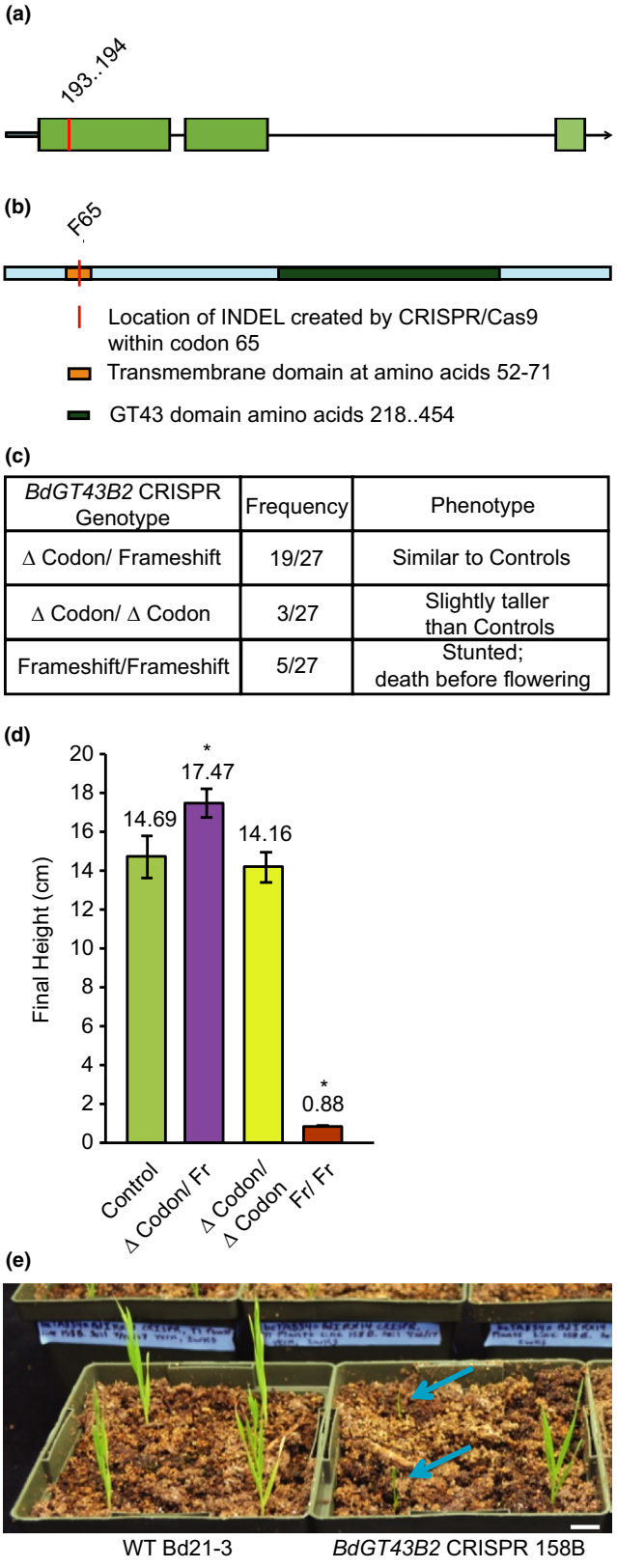

BdGT43B2 CRISPR Genotype	Frequency	Phenotype
Δ Codon/ Frameshift	19/27	Similar to Controls
Δ Codon/ Δ Codon	3/27	Slightly taller than Controls
Frameshift/Frameshift	5/27	Stunted; death before flowering

FIGURE 1 *BdGT43B2* gene and protein model; frequency of CRISPR/Cas9-induced mutations. (a) *BdGT43B2* gene model. *BdGT43B2* has a 337 bp 5′UTR, followed by a 848 bp Exon 1, 102 bp Intron 1, 549 bp Exon 2, 1,868 bp Intron 2, 193 bp Exon 3, and a 364 bp 3′UTR. The *BdGT43B2* guide RNA for CRISPR/Cas9-mediated genome editing was located on the reverse strand at position 547..528 of the B*dGT43B2* genomic sequence, downstream 210..191 of the + 1 ATG of the cds. The location of the double-stranded break (DSB) was between nucleotides 193..194 of the cds, within exon 1. (b) BdGT43B2 amino acid model. The site of the DSB is within the transmembrane domain located at amino acids 52..71. The DSB site will interrupt F65 within the transmembrane domain. (c) Summary of genotypes of *BdGT43B2* CRISPR Cas9 initial regenerants. (d) Final height data were collected from T1 progeny of the initial *BdGT43B2* regenerants. Two experimental replicates were performed and data combined. For the transgenic controls, 4 eGFP CRISPR transgenic lines were planted, and four individuals per line were genotyped in each of the two plantings, for a total $n = 32$. For the Δ Codon/Frameshift genotyped plants, $n = 90$. For the Δ Codon/Δ Codon plants, $n = 27$. For the Frameshift/Frameshift genotyped plants, $n = 8$. This relatively low number of plants genotyped as Frameshift/Frameshift inheriting individuals is likely due to this genotype affecting effective germination and elongation of seedlings. (e) Subset of *BdGT43B2* CRISPR Line 158B T1 progeny segregating for stunting (stunted individuals indicated with black arrows), in comparison to WT Bd21-3 controls. Scale bar is 1 cm

xylan levels and improved straw digestibility, but few effects on plant growth (Whitehead et al., 2018).

Here, we sought to investigate the importance of xylan production to grass growth and development, particularly to ascertain the importance of xylan synthesis to early seedling development differed in grasses as compared to the model dicot species *Arabidopsis thaliana*. We chose BdGT43B2/*Bradi1g33320*, the *Brachypodium distachyon* ortholog of IRX14 and TaGT43-4 (Jiang et al., 2016), as a target to probe xylan biosynthesis because its proposed function mainly as a scaffolding protein implies its necessity for the assembly of a functional XSC. We used CRISPR/Cas9 mutagenesis to create functional knockout mutations in *BdGT43B2*, and also generated artificial microRNA (amiRNA) knockdown lines targeting *BdGT43B2*. CRISPR mutant plants were stunted and died as seedlings. Fluorescent immunolabeling of CRISPR knockout and amiRNA knockdown plants indicated a reduction in xylan, whereas biochemical quantitation demonstrated a small xylose reduction in the amiRNA lines, and a significant reduction of digestible xylan in the CRISPR knockout lines. Together, these data point to the conclusions that *BdGT43B2* is involved in xylan biosynthesis, and the presence of xylan in the primary cell walls of Brachypodium seedlings is essential for normal growth and development.

2 | METHODS

2.1 | Design and cloning of *BdGT43B2* CRISPR construct

A guide RNA targeting *BdGT43B2* for CRISPR-Cas9 targeted gene mutation was designed following (Xie, Minkenberg, & Yang, 2014; Xie, Zhang, & Yang, 2014). Guide RNA candidates targeting *BdGT43B2* (*Bradi1g33320*) were identified using the CRISPR-Plant database (Xie, Minkenberg, et al., 2014; Xie, Zhang, et al., 2014) (genome.arizona.edu/crispr). A gRNA target site with a low probability score of mis-targeting was chosen near the 5′ end of the coding sequence.

Oligos pCTA2387 and pCTA2383 (Table S1) were designed to create a single gRNA targeting a double-stranded break repair in *BdGT43B2* between nucleotides 193 and 194 of the coding sequence, which corresponds to altering the amino acid sequence beginning at amino acid F65 (Figure 1). A control guide RNA sequence targeting eGFP was designed using pCTA2390 and pCTA2391 (Table S1) to create a transgenic negative control; this sequence was checked for a low probability of off-target effects against the Bd21-3 genome. The sequences GGCA and AAAC were added to the 5′ ends of the forward and reverse primers, respectively, as cloning adapters to allow BsaI cloning into the transformation vector pRGEB32. One microliter each of 100 μM forward and reverse oligos were mixed with 7 μl of sterile water and 1 μl of 1× T4 DNA ligase buffer and incubated for 60 min at 37°C then 10 min at 95°C, and cooled to 25°C at 0.1°C/s. A 1:200 dilution of the oligo duplex was then ligated to BsaI digested pRGEB32 (Xie, Minkenberg, & Yang, 2015) vector as follows: 1.0 μl of 63.0 ng/μl BsaI digested pRGEB32, 1.0 μl of 1:200 diluted oligo duplex, 0.5 μl of 10× T4 DNA ligase buffer, 1.0 μl of T4 DNA ligase, 1.5 μl of sterile water. This 5 μl ligation was incubated overnight at 4°C with a heated lid. One microliter of the ligation product was transformed into TOP10 cells and selected on LB + 60 μg/ml kanamycin. Clones were miniprepped and sequenced using the M13R (−48) primer.

2.2 | Transformation of Bd21-3 embryogenic callus and subsequent regeneration

Embryos were dissected from wild-type Bd21-3 immature seeds and placed on callus induction medium, pH 5.8 (Bragg, Anderton, Nieu, & Vogel, 2015) containing 2.5 μg/ml 2,4-D (Sigma D7299) to generate embryogenic callus. The *Agrobacterium tumefaciens* strain AGL-1 was transformed via electroporation and selected using antibiotic resistance specific for the plasmid being introduced. Transformation and regeneration methods were performed as described (Bragg et al., 2015; Vogel & Hill, 2008); media were supplemented with 40 Units/ml Hygromycin B (DOT Scientific). The only difference with the (Bragg et al., 2015) protocol was that timentin was included at 150 μg/ml final concentration in the callus selection media, pH 5.8 (the same recipe as callus induction media, but including 40 μg/ml Hygromycin and 150 μg/ml timentin), and in the Regeneration media, pH 5.8 (Bragg et al., 2015) In instances where inadequate rooting occurred while plantlets were incubated on 1× Murashige and Skoog (pH 5.7) medium in magenta boxes, 2 mg/L NAA rooting hormone (Caisson Labs NSL01) was added to the MS medium.

2.3 | Genotyping of *BdGT43B2* CRISPR plants

Genomic DNA was isolated from leaf disks of juvenile *BdGT43B2* CRISPR plants using the Sigma-Aldrich Plant Extract n Amp DNA isolation kit according to manufacturer's instructions. PCR amplification products using primers pCTA2525 and pCTA2526 were sequenced and screened for the presence of an insertion or deletion near the double-stranded break (DSB) site.

A second genotyping method was used to validate indel size when genotyping bi-allelic individuals. PCR through the DSB site was performed using a forward primer with a 5' 6-FAM fluorescent adapter (pCTA2542, Table S1), and products were sized via fragment analysis separation using a 3,730 XL DNA sequencer at the Penn State Genomics Core Facility. Data analysis was performed using Thermo Fisher's Peak Scanner Program. By comparing the sizes of peaks to the single peak generated control plants, the number of bases inserted or deleted could be independently verified in heterozygous or bi-allelic individuals, which would be difficult to do by sequencing due to the varying shifts in sequencing peaks produced by different mutant alleles.

2.4 | Plant growth

Transgenic plants were grown in a 50:50 mix of Sungro Redi-Earth Seedling and Plug Mix:Metromix 510 in 10 cm pots. Plants were grown in 20 hr light/4 hr dark cycles at 25°C at a light intensity of 150–200 μmol m^{-2} s^{-1} under 20%–40% humidity. For growth assays of adult plants, seedlings were germinated on ½ MS + 0% sucrose + 40 μg/ml Hygromycin for 4 days at 22°C, then transplanted to 4 L pots containing the above soil mix and grown in a greenhouse under 16 hr light per day with a light intensity of 150 μmol m^{-2} s^{-1} until senescence, when final height was measured.

2.5 | Immunofluorescence labeling

Seeds were surface sterilized, stratified for 3 days in the dark at 4 °C, and germinated on ½ MS plates with 40 μg/ml hygromycin for 3 days in the dark. Etiolated seedling shoots were excised 1 mm above the connection point to the seed, and fixed for 24 hr at 4 °C in PEM buffer (0.1 M PIPES, 2 mM EGTA, 1 mM MgSO4, pH 7.0) + 4% paraformaldehyde. Shoots were rinsed in PEM buffer, then dehydrated in an ethanol series consisting of 30%, 50%, 70%, and 100% ethanol for 30 min each prior to an overnight 100% ethanol incubation. Shoots were then infiltrated with 10%, 20%, 30%, 50%, 70%, and 90% LR White resin in 100% ethanol (v/v) for 1 hr each at room temperature. This was followed by three overnight infiltrations in 100% LR white at 4 °C. Shoots were placed into gelatin capsules containing 100% LR white, and polymerized for two days at 65 °C. After polymerization, blockfaces were prepared from basal sections of the embedded coleoptiles, and 2-μm transverse sections of the mesocotyl regions were prepared using a Leica UC6 ultramicrotome (Buffalo Grove, Illinois) with a glass knife. These 2-μm sections were collected and dried onto positively charged glass slides (Shandon SuperFrost Plus Positively Charged Microscope Slides, Thermo Scientific).

For immunofluorescence labeling, sections were outlined on the surface of the slides using a PAP pen (Ted Pella, Inc.) to entrap

hybridization and washing solutions. Sections were blocked for 1 hr in PBS buffer + 5% milk powder. The blocking solution was then removed and sections were incubated overnight in humidified chambers at room temperature in blocking solution with or without 1:10 diluted LM11 primary antibody (PlantProbes). The next day, sections were washed three times with PBS buffer, and incubated with Alexa 488 goat-anti-rat IgG secondary antibody diluted 1:100 in blocking buffer for 2 hr at room temperature in the dark. Sections were rinsed three times with PBS buffer, then stained for 30 min using 0.1% (w/v) S4B (Pontamine Fast Scarlet 4B, available from Sigma-Aldrich under the synonym Direct Red 23, catalog # 212490) to stain cellulose.

2.6 | Immunofluorescence imaging and data analysis

Images were collected on a Zeiss Cell Observer *SD* microscope with a Yokogawa CSU-X1 spinning disk head. Images were collected using 10× air (NA and 20× air objectives; the 10× objective was used to view the entire transverse section in the field of view to look for morphological differences, while the 20× objective was used for the immunofluorescence quantitation measurements. A 488 nm excitation laser and a 525/50 nm emission filter were used to detect Alexa Fluor 488 signals, and a 561 nm excitation laser and a 617/73 nm emission filter were used to detect S4B signals.

Maximum projections were created from each Z-stack. The maximum projections were background subtracted using a 50-pixel sliding paraboloid. Because experiments performed on different days showed variation in the intensity of secondary antibody and S4B fluorescence, the parameters that allowed optimal imaging of the controls were not identical. Therefore, when compiling fluorescence intensity (RawIntDen/Area) values across multiple experiments, data were first normalized to the transgenic controls (eGFP amiRNA or eGFP CRISPR) imaged within the same experiment. For graphing, average normalized (RawIntDen/Area) values per transgenic line were used. Three normalized technical replicates across three biological replicates per transgenic line were compiled for $n = 9$ per transgenic line. Student's *t*-tests (two-tailed, type 3) were used to compare each transgenic line to controls.

2.7 | Cell wall extraction and methanolic HCL/TFA hydrolysis

Shoots were flash frozen in liquid nitrogen upon excision from etiolated seedlings. Frozen etiolated shoots were ground under liquid nitrogen using mortar and pestle, and the powder was transferred to 50-ml Falcon tube containing 30 ml of 1:1 chloroform:methanol. Samples were rocked for 1 hr at room temperature, centrifuged at 3,242 *g* for 10 min, and the supernatant was removed. This step was repeated prior to incubating the cell wall material three times in 30 ml 70% ethanol for 1 hr each with centrifugation between each wash. After the last 70% ethanol wash and spin, cell wall material was resuspended in 5 ml acetone, centrifuged, acetone was removed, and the pellet was allowed to dry overnight in a chemical fume hood. Alcohol insoluble residue (AIR) pellets were resuspended in 2.5 ml water and freeze-dried to obtain cell wall material that was fluffy, and 2–3 mg of each sample was weighed and transferred to Sarstedt tubes for methanolic HCl/TFA hydrolysis.

AIR samples were treated with 1 ml of 2 M HCl in methanol for 16 hr at 80 °C. Samples were cooled briefly on ice, centrifuged, and the liquid evaporated under a gentle stream of air. For each sample, 1 ml of 2 M TFA was added, and the samples were incubated for 1 hr at 121 °C. The samples were cooled on ice, and centrifuged at 8,000 *g* for 5 min. The supernatant was transferred to new Sarstedt tubes and the liquid was evaporated under a gentle stream of air. The dried hydrolyzed sugars were then dissolved in 1 ml ddH_2O and filtered through a 0.22 μm pore size, 4 mm diameter low binding Durapore (PVDF) membrane filter (Millex-GV) and passed through a DIONEX OnGuard II RP 1 cc cartridge. Passing quantities of sugars through the RP cartridge resulted in a loss of 7% sugar loss by total sugar quantitation assay, but this was determined to be acceptable because the subsequent quantitation of each monosaccharide present in the hydrolyzed AIR samples is expressed in molar ratios.

2.8 | Monosaccharide analysis

Monosaccharide analysis was performed as in (Xiao, Somerville, & Anderson, 2014). A total of 20 μL of each sample was injected into a high-pressure anion exchange chromatography system with pulsed-amperometric detection using a CarboPac PA20 guard (3 × 30 mm) and column (3 × 150 mm; Dionex ICS-5000; Thermo Scientific). Elution steps were 10% 100 mM NaOH for 15 min, followed by a 0–100% gradient of 100 mM NaOH in 100 mM NaOAc for 20 min. Sugar monosaccharide peaks in the samples were quantified using Fuc, Rha, Ara, Gal, Glc, Xyl, GalA, and GlcA standards at 1 mg/ml. Chemicals were purchased from Sigma-Aldrich, and eluents were from Thermo Scientific. Three technical replicates were performed for each of three biological replicates per transgenic line.

2.9 | Xylan analysis by pace

To determine xylan structure, xylan in alcohol insoluble residue (AIR) was solubilized with 4 M NaOH and reducing ends were reduced with 10 mg/ml $NaBH_4$ in 0.5 M NaOH for 2 hr at room temperature. The reaction was terminated by adjusting to pH 5.5 with glacial acetic acid on ice. Borates were removed with 10% acetic acid in methanol and samples were desalted by passing through a PD-10 column (GE Healthcare). Xylan was digested using GH11 endo-β-1,4-xylanase NpGH11A from *Neocallimastix patriciarum* (Gilbert, Hazlewood, Laurie, Orpin, & Xue, 1992) at 21°C under constant shaking for 24 hr. GH11 enzyme was removed from the reaction mixture with filtration using Nanosep system (molecular weight cutoff of 10 kDa, Pall, New York, USA). The oligosaccharides were further digested with GH115 α-glucuronidase BoGH115 from *Bacteroides ovatus* (Rogowski et al., 2014) (gift from Harry Gilbert) and GH3

β-1,4 xylosidase TrGH3 from *Trichoderma reesei* (Margolles-Clark, Tenkanen, Nakari-Setälä, & Penttilä, 1996) (gift from Novozymes). All enzymes were added at a final concentration of 2 μM and incubated at 21°C under constant shaking for 24 hr.

Derivatization of digested carbohydrates was performed according to previously developed protocols (Mortimer, 2017). Carbohydrate electrophoresis and PACE gel scanning and quantification were performed as described by Goubet et al. (2009), Goubet, Jackson, Deery, & Dupree (2002). Control experiments without substrates or enzymes were performed under the same conditions to identify any non-specific compounds in the enzymes, polysaccharides/cell walls or labeling reagents.

For PACE, 3 mg of AIR was used. The samples were reduced and desalted, and samples were then split into 6 sub-samples (i.e., corresponding to 0.5 mg of AIR) prior to enzyme hydrolysis. Oligosaccharide products were then labeled and resuspended in 50 μl 3 M urea. Eight microliter of these resuspensions were then loaded on the gel. Therefore, material corresponding to about 80 μg of AIR was loaded into each lane of the polyacrylamide gel.

2.10 | Cell dimension measurements

Seeds were surface sterilized and plated on ½ MS + 1% sucrose germination plates. Seeds were allowed to stratify for 4 days in the dark at 4°C, followed by 4 days of growth under constant light at 22°C. Plates were then scanned prior to the cotyledenous leaves of seedlings being dissected out of the surrounding coleoptile in mutant seedlings. This dissection step was not necessary for control seedlings, as all monocotyledonous leaves had emerged from the coleoptile by 4 days. Monocotyledonous leaves were briefly dipped in 0.01% Triton X-100, rinsed with water, stained with 0.1 mg/ml propidium iodide in water (Molecular Probes) for 5 min, and imaged on a spinning disk confocal microscope (see above). ImageJ was used to measure the length and width of a minimum of 334 cells per genotype from 7–12 biological replicates per genotype. Cell lengths and widths were statistically compared using Student's two-tailed, type 3 *t*-tests.

2.11 | Design and cloning of *BdGT43B2* amiRNA construct

An amiRNA targeting *BdGT43B2* (*Bradi1g33320*) was designed using the James Carrington lab Plant Small RNA Maker Suite lab application (http://p-sams.carringtonlab.org), filtering amiRNA candidate sequences to remove those with potential off-targets in the genome. Cloning adapter sequences consisting of "CTTGT" and "CATGG" were added to the 5′ ends of forward and reverse primers, creating primers pCTA2295 and pCTA2296 (Table S1), respectively, to allow cloning of the annealed primer pairs into the pH7WG2B-OsMIR390 B/C vector. Each primer was dissolved at 100 μM in sterile water. Two μl of each 100 μM primer was added to 46 μl of oligo Annealing Buffer ((60 mM Tris-HCL (pH 7.5), 500 mM NaCl, 60 mM $MgCl_2$, 10 mM DTT)), mixed and denatured for 5 min at 94°C. The reaction was then slowly cooled at a rate of 0.05°C/s down to 20°C to allow primer annealing. Ligation was performed at 16°C overnight with 1 μl of BsaI digested and purified vector, 1 μl of 1:10 diluted annealed oligos, 2 μl 10× T4 DNA ligase buffer, 1 μl 400U/μl T4 DNA ligase, and 15 μl sterile water. Two μl of the ligation reaction was transformed into the Top10 strain of *E. coli*, and colonies were selected using 100 μg/ml spectinomycin. After plasmid purification, clones were sequenced using attB1 and attB2 sequencing primers (Table S1). To create a transgenic negative control plasmid, an amiRNA sequence was designed targeting eGFP using primers pCTA2388 and pCTA2389 (Table S1), which was not present in WT Bd21-3.

2.12 | Quantitative RT-PCR (QRT-PCR)

Juvenile leaves were collected 27 days after germination, before the transition to flowering. Leaves were frozen in liquid nitrogen, ground using a mortar and pestle, and total RNA extracted using the Machery-Nagel NucleoSpin RNA Plant Kit (www.mn-net.com) according to manufacturer's instructions, including on-column DNA digestion. A total of 0.5 μg of RNA was reverse-transcribed using a qScript cDNA SuperMix kit (Quanta BioSciences) according to manufacturer's instructions. From the first-strand cDNA reactions, 1:5 dilutions were used for qRT-PCR, along with 5 ng of WT Bd21-3 RNA as a no reverse-transcription control, as recommended in the Quanta qScript cDNA SuperMix protocol.

qRT-PCR primers were designed using the Primer-Blast program (ncbi.nlm.nih.gov), which uses the Primer 3 algorithm. Primers were designed to amplify 80–100 bp products, in locations spanning exon:exon junctions. The Perfecta SYBR Green FastMix with ROX (Quanta Biosciences) was used with *BdGT43B2* transcript-specific primers pCTA2677 and pCTA2678 (Table S1) to amplify 1 μl of 1:5 diluted cDNA in a 10 μl PCR reaction containing primers at final concentrations of 300 nM. Thermal cycling conditions were: 95°C 2 min, 40 cycles of (95°C 10 s, 60°C 30 s), followed by a melting curve analysis of 95°C 15 s, 60°C 1 min, 95°C 15 s. PCR was performed on a StepOne Plus Real-Time PCR machine (Applied Biosystems). Ct values were collected at the end of each 60-s annealing-extension step. *BdUBC18* (*Bradi4g00660*) was amplified as the reference gene using pCTA2177 and pCTA2178 (Table S1), and relative expression was calculated using the ΔΔCt method. Three technical replicates of three biological replicates were performed. qRT-PCR of fellow *GT43* members *BdGT43B1* (*Bradi5g24290*) and *BdGT43A2* (*Bradi5g02350*) was performed on the same cDNA samples using pCTA2773/pCTA2774 and pCTA2803/pCTA2804, respectively (Table S1). This was done to determine where these genes were expressed in a compensatory manner in the *BdGT43B2* amiRNA plants.

2.13 | Statistical analysis

Statistical analysis of height data was performed by comparison of mutants to the appropriate transgenic control by Student's *t*-test,

using a two-tailed, type 3 test. Statistical analysis of normalized Fluorescence intensity/Area was also performed by Student's *t*-test, using a two-tailed, type 3 test. Analysis of predicted to expected phenotypic frequencies of CRISPR etiolated shoot and root stunting was performed using Chi-square analysis. Analysis of cell dimensions was performed by Student's *t*-test, using a two-tailed, type 3 test.

3 | RESULTS

3.1 | Induction of mutations in *BdGT43B2* via CRISPR/Cas9 genome editing

Based on sequence similarity to the wheat Xylan Synthase Complex scaffold protein *TaGT43-4* (Jiang et al., 2016) related to Arabidopsis IRX14, we chose *BdGT43B2* (*Bradi1g33320*) as a target for genome editing-mediated knockout. A guide RNA sequence was designed to target Cas9 between nucleotides 193 and 194 of the *BdGT43B2* cds, within exon 1 (Figure 1a). Insertions or deletions at this location interrupted the codon for Phe65, within the transmembrane domain, upstream of the GT43 domain (Figure 1b). In 19/27 transgenic lines, one allele of *BdGT43B2* exhibited a frameshift-inducing 1 or 2 nt indel, whereas the other allele showed an indel in a multiple of three nucleotides. In 5/27 transgenic plants, frameshift-inducing mutations were detected on both alleles of the gene. All five of these transgenic plants were severely stunted and died within 2 weeks of transplantation (Figure 1c). The mutated DNA sequence surrounding the double-stranded break site of these five Fr/Fr mutants is provided (Table 1). Lastly, in 3/27 transgenic lines regenerated, both *BdGT43B2* alleles had a multiple of three nucleotides deleted, maintaining the translation frame with the loss of one or more codons (Figure 1c). Notably, none of the *BdGT43B2* CRISPR plants regenerated from tissue culture showed the presence of a wild-type *BdGT43B2* allele, indicating an editing efficiency of 100%.

3.2 | *BdGT43B2* frameshift/frameshift CRISPR mutants show severe growth defects and die prematurely

Although there is often variation in height among transgenic Brachypodium plants coming out of tissue culture, the fact that all five transgenic lines that had a frameshift-inducing mutation on both alleles of *BdGT43B2* were severely stunted and died within two weeks after transplantation to soil indicated that *BdGT43B2* is likely to be essential for survival in Brachypodium. *BdGT43B2* Frameshift/Frameshift (Fr/Fr) plants grew an average of 1.84 cm tall (*SD* = 0.83 cm) before death, which occurred before transition to flowering. In contrast, all other *BdGT43B2* CRISPR and eGFP CRISPR transgenic regenerated plants did not exhibit stunting. Plants initially coming out of tissue culture can exhibit non-reproducible phenotypes due to the hormone treatments they receive during regeneration. Therefore, height data were collected from the progeny of heterozygous T0 regenerants containing one Fr allele that were allowed to self-pollinate, of which about 1/4 should be Fr/Fr. T1 progeny were grown in two experimental replicates (Figure 1d). Of the statistically significant differences in final height observed, *BdGT43B2* Fr/Fr plants grew only 6% as tall as transgenic controls (n = 8 plants/genotype, $p = 3.77 \times 10^{-14}$, *t*-test), whereas Δ Codon/Frameshift plants grew 119% as tall as transgenic controls (n = 90 plants/genotype, p = .04, *t*-test). A subset of *BdGT43B2* CRISPR

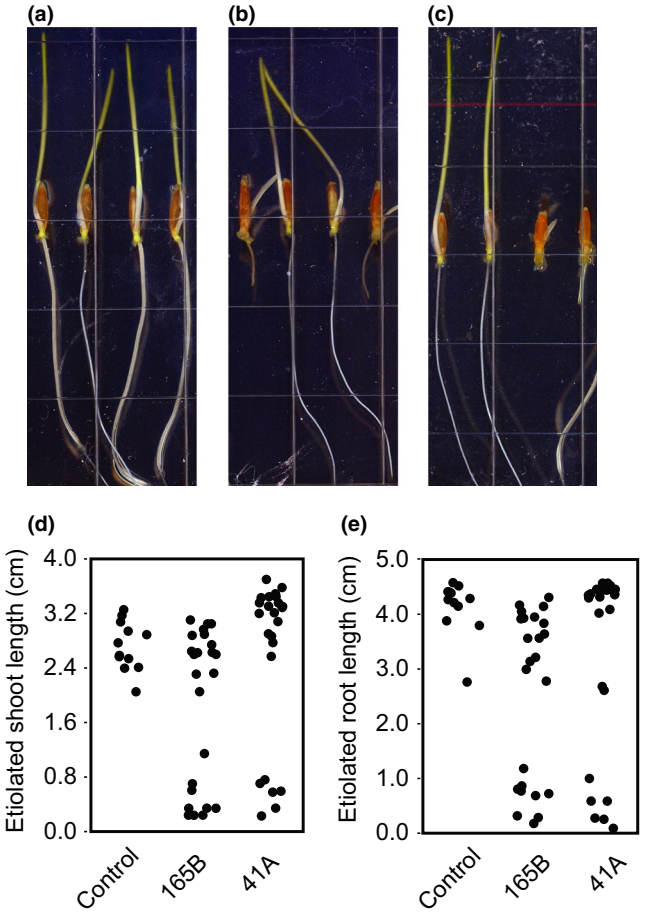

FIGURE 2 *BdGT43B2* homozygous CRISPR frameshift knockout mutants exhibit seedling root and shoot stunting. Seedlings of the *BdGT43B2* CRISPR mutants were germinated without hygromycin selection because all CRISPR individuals had an INDEL on each *BdGT43B2* allele. Therefore, the transgenic control was germinated similarly. T1 plants which were genotyped as Δ Codon/Frameshift at the *BdGT43B2* gene were allowed to self-pollinate, the T2 seed collected, and germinated in this assay. (a) eGFP CRISPR transgenic control line 71A T2 seedlings. The eGFP CRISPR etiolated seedlings grew shoots and roots which did not segregate in length, and were similar in length to WT seedlings grown on ½ MS plates + 1% sucrose for 4 days (data not shown). (b) *BdGT43B2* CRISPR Line 165B T2 seedlings. These seedlings segregated for both shoot and root length, with 9/24 exhibiting extreme stunting. (c) *BdGT43B2* CRISPR Line 41A T2 seedlings. These seedlings also segregated for shoot and root length, with 6/24 exhibiting extreme stunting. (d) Jitter plot of the lengths (cm) of etiolated shoots four days after germination, displaying the segregation ratios with the 165B and 41A lines. (e) Jitter plot of the lengths (cm) of etiolated roots four days after germination, displaying the segregation of root length within the 165B and 41A T2 individuals

line 158B T1 progeny showed stunting in comparison to wild-type Bd21-3 plants (Figure 1e).

3.3 | Etiolated *BdGT43B2* frameshift/frameshift seedlings exhibit stunted shoots and roots

BdGT43B2 CRISPR lines 41A and 165B were chosen for further phenotypic analysis. Transgenic line 41A had 3 nt deleted on one *BdGT43B2* allele, and 5 nt deleted on the other allele in the T0 generation. Transgenic line 165B had 6 nt deleted on one *BdGT43B2* allele, and 1 nt inserted on the other allele in the T0 generation. Therefore, when each of these plants self-pollinated, 1/4 of the progeny inherited a frameshift-inducing mutation on both *BdGT43B2* alleles, and were stunted and died before flowering. Thus, a propagating population of *BdGT43B2* CRISPR homozygous frameshift mutants could not be obtained, but 1/4 of the seed produced by bi-allelic plants Fr/Fr. *BdGT43B2* CRISPR Fr/Fr plants could be analyzed as seedlings before they died. T2 seeds of eGFP CRISPR control line 71A, *BdGT43B2* CRISPR line 165B, and the *BdGT43B2* CRISPR line 41A were germinated under etiolated conditions on 1/2 MS + 1% sucrose plates for 4 days. eGFP CRISPR seedlings grew shoots and roots that did not vary widely in length (Figure 2a,d,e), whereas *BdGT43B2* CRISPR seedlings segregated for shoot and root length (Figure 2b–e). Segregation patterns of seedling stunting (9/24 for line 165B, and 6/24 for line 41A) were consistent with Mendelian inheritance of frameshift alleles ($p > .05$, χ^2 analysis).

3.4 | LM11 immunolabeling of xylan is reduced in *BdGT43B2* CRISPR FR/FR seedlings

To assess the presence of xylan in *BdGT43B2* CRISPR Fr/Fr seedlings, 2 µm sections of 4 dag (days after germination) etiolated seedling shoots were immunolabeled using the LM11 primary antibody, which binds to xylan with varying degrees of side group substitution (Ruprecht et al., 2017), then stained with the cellulose dye, S4B (Anderson, Carroll, Akhmetova, & Somerville, 2010), to reveal cell wall areas. Strong reductions in LM11 immunolabeling were observed in *BdGT43B2* CRISPR lines 165B and 41A relative to the eGFP CRISPR control (Figure 3a). CRISPR lines 165B and 41A showed 88% and 98% reductions in (Immunolabeling Fluorescence: Wall Area) ratios relative to controls (Figure 3b; $p < .05$, *t*-test). In contrast, S4B staining of cellulose was slightly higher in *BdGT43B2* CRISPR Fr/Fr seedlings than in eGFP CRISPR controls (Figure 3c), resulting in lower LM11:S4B intensity ratios in Fr/Fr seedlings (Figure 3d).

In control seedlings, the strongest LM11 labeling lay within the vascular cylinder, or central tracheary element, of the cross sectioned mesocotyl, of which only the central portion of which is shown in Figure 3. The strongest LM11 labeling was in pericycle cells, which consist of both parenchyma and schlerenchyma cells. The parenchyma cells that exist in the pericycle are non-vascular, and both they and schlerenchyma cells in the pericycle serve to provide structural support to the plant. Therefore, depletion of xylan in non-vascular cells of the *BdGT43B2* CRISPR mutants might reduce wall structural integrity, but not affect water transport, but nonetheless result in lethality. Consistent with this hypothesis, no major defects in vascular cell shape were observed in Fr/Fr seedlings (Figure 3).

Morphological differences were qualitatively observed in the *BdGT43B2* CRISPR mesocotyl sections in comparison to the eGFP CRISPR transgenic control and WT. The diameter of the vascular cylinder appeared decreased in the *BdGT43B2* CRISPR seedling mesocotyl sections in comparison to the controls. Further, the cells within the vascular cylinder appear to be more tightly packed, and to have thicker cell walls (Figure 3a).

FIGURE 3 Immunolabeling of xylan in *BdGT43B2* CRISPR etiolated mesocotyls. Cross sections of 4 days old seedling mesocotyls. The central region is the vascular cylinder, also known as the central xylem tracheary element. vc = vascular cylinder; c = cortex; xv = xylem vessel; en = endoderm; ph = phloem; pc = pericycle; Od = Outer descending scutellar trace (Raju & Steeves, 1998). (a) Mesocotyl cross sections of etiolated shoots from the *BdGT43B2* CRISPR lines 165B and 41A were subjected to LM11 immunolabeling of xylan. The eGFP CRISPR line 71A served as the transgenic control. Excitation using 488 nm laser allowed indirect quantitation of xylan in Ch1, while imaging of cellulose using 0.1% S4B staining allowed imaging of all cell walls in Ch2. The two images merged is shown in the 3rd column. S4B images were increased in contrast by 0.4% saturated pixels across all samples for visualization purposes, but unadulterated images were used for fluorescence quantitation. One can see in these representative images that both line 165B and 41A had much less fluorescent detection of xylan in comparison to the transgenic control. (b) Mean (Fluorescence Intensity/Area) of three biological replicates per transgenic line, normalized to the transgenic control. Lines 165B and 41A showed 12% and 2% of the transgenic control's normalized Fluorescence Intensity/ Area, which was a statistically significant difference from the control using Student's *t*-test (two-tailed, type 3) with $n = 9$ per transgenic line. (c) S4B Fluorescence Intensity/Area, normalized to the transgenic control. Lines 165B and 41A showed somewhat higher values compared to the transgenic control, with only the difference between line 41A and the transgenic control being significant ($p < .05$). Statistical analysis was performed as described in (b). (d) Ratio of Normalized LM11 (Fluorescence Intensity/Area) to Normalized S4B (Fluorescence Intensity/Area). Although either a decrease in the LM11 (Fluorescence Intensity/Area) numerator or an increase in the S4B (Fluorescence Intensity/Area) denominator of the ratio between the two would cause a decrease in the ratio's value, one can clearly see that there was a much greater decrease in LM11 Fluorescence Intensity/Area than the amount of increase in the S4B Fluorescence Intensity/Area, and therefore that the decrease in LM11 (Fluorescence Intensity/Area) plays a much bigger role in the change of the LM11 to S4B normalized Fluorescence Ratio. Three technical replicates per each of three biological replicates were performed. Scale bar equals 50 µm. Images were captured using 250 ms exposure, 1,000 EM gain, 2% 488 nm laser power, 100% 561 nm laser power. Asterisks in graphs b, c, and d indicate statistical significance using Student's *t*-test (2-tailed, type 3) at p< .05

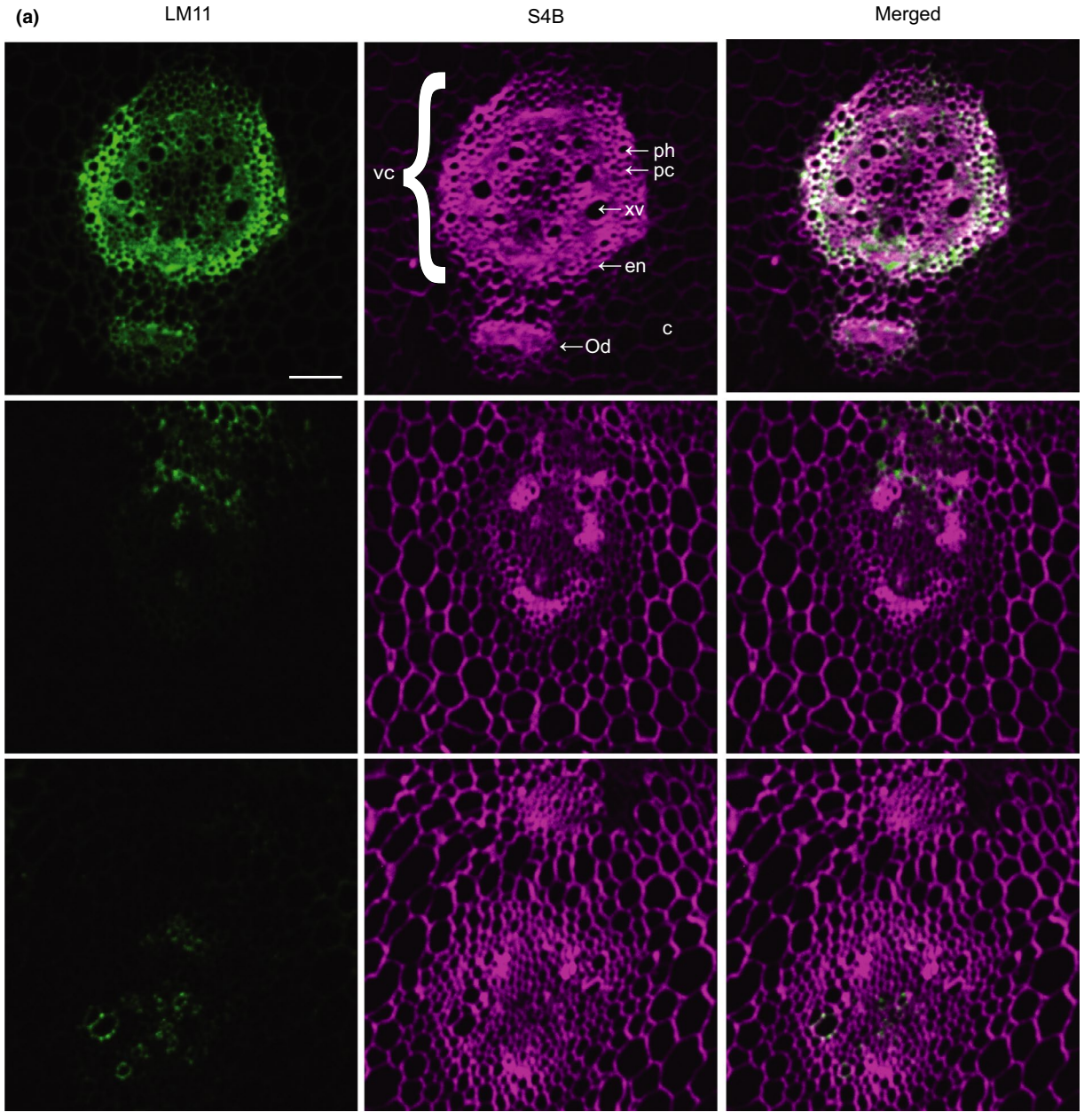
(a)
LM11
S4B
Merged
vc
ph
pc
xv
en
c
Od
Transgenic Control CRISPR
BdGT43B2 CRISPR Line 165B
BdGT43B2 CRISPR Line 41A

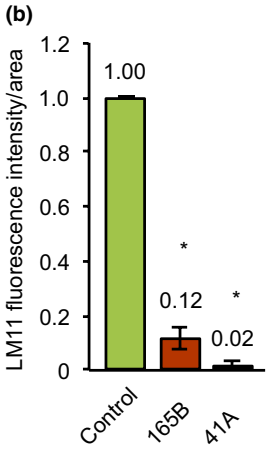
(b)
LM11 fluorescence intensity/area
1.00
0.12
0.02
*
*
Control
165B
41A

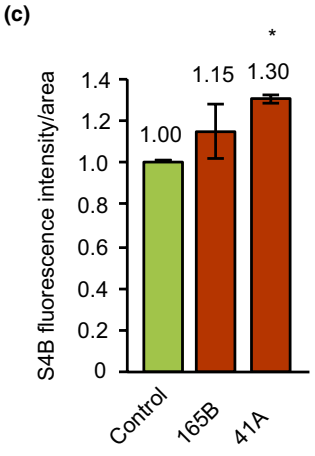
(c)
S4B fluorescence intensity/area
1.00
1.15
1.30
*
Control
165B
41A

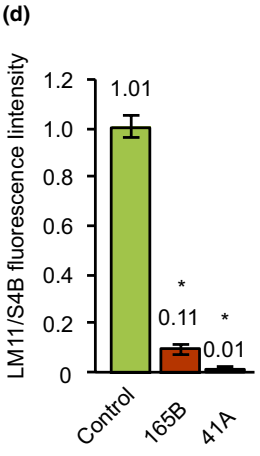
(d)
LM11/S4B fluorescence intensity
1.01
0.11
0.01
*
*
Control
165B
41A

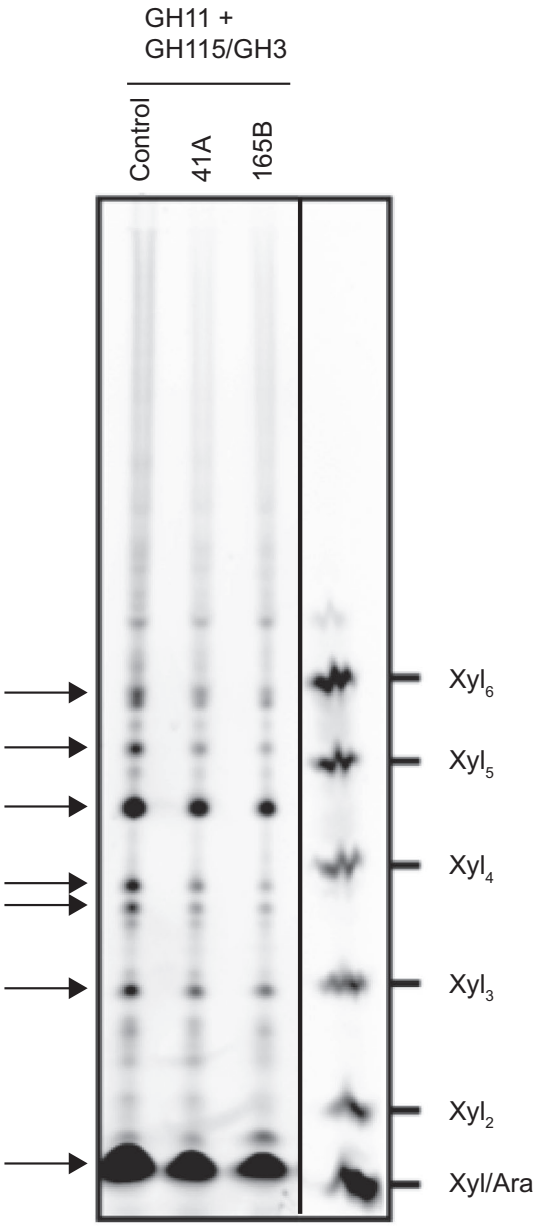

FIGURE 4 Xylan structure in etiolated seedlings from transgenic control and CRISPR knockout plants. AIR from etiolated seedlings of transgenic control and *BdGT43B2* CRISPR 41A and 165B lines was digested with xylanase *Np*GH11A, followed by GH115 α-glucuronidase and GH3 β-1,4 xylosidase and analyzed by PACE. Markers Xyl/Ara to Xyl_6 and previously characterized oligosaccharides $XD^{2,3}XX$, XA^3XX and XA^3X are shown. Bands marked with asterisks are novel arabinosylated xylo-oligosaccharide structures

3.5 | Xylan digestion products are reduced in *BdGT43B2* CRISPR seedlings

To investigate the biochemical basis for stunting and premature death in the *BdGT43B2* CRISPR mutants, polysaccharide analysis by carbohydrate electrophoresis (PACE) (Goubet et al., 2002) was employed (Figure 4). Hydrolysis of eGFP CRISPR control AIR released mainly Xyl, $XD^{2,3}XX$ (Xyl [Beta1,2 Xyl-alpha1,3-Araf-]Xyl-Xyl-Xyl), XA^3XX (Xyl [alpha1,3-Araf-]Xyl-Xyl-Xyl) (Tryfona et al., 2019) and some further uncharacterized oligosaccharides. Notably, the hydrolysis of both *BdGT43B2* CRISPR line AIR (41A and 165B) showed a clear decrease in the intensity of all bands, indicating the mutants contained reduced amounts of digestible xylan.

3.6 | *BdGT43B2* CRISPR seedlings exhibit diminished cell expansion

To determine whether *BdGT43B2* CRISPR Fr/Fr seedlings were stunted due to diminished cell expansion, cotyledonous leaves of 4 dag light-grown seedlings were stained with propidium iodide to reveal cell outlines and imaged. As shown in Figure 5, BdGT43B2 CRISPR line 49A had a significant reduction in both cell length and width, whereas line 158B only showed a reduction in cell length, in comparison to controls. Trichome number and size were also reduced, suggesting that xylan reduction also affects expansion of this cell type.

3.7 | *BdGT43B2* amiRNA plants exhibit moderate stunting as seedlings, but appear normal as adults

Because we suspected that a complete loss of BdGT43B2 protein production is lethal, a strategy to knock down the expression of BdGT43B2 was also employed. A 21 nt artificial microRNA complementary to nucleotides 1,269 to 1,288 in exon 2 of the *BdGT43B2* cds was designed, cloned into the pH7WG2B-OsMIR390 B/C vector, and transformed into WT Bd21-3. Recall that when designing amiRNAs, the amiRNA sequence is 21 nt long, but includes a 1 nt mismatch; therefore, only 20 of 21 nucleotides will match target position numbers. Eight independent *BdGT43B2* amiRNA transgenic lines were obtained, with lines 86A (19% *BdGT43B2* expression remaining) and 12A (23% *BdGT43B2* expression remaining) showing the greatest reduction of *BdGT43B2* expression in qRT-PCR experiments (Figure 6a). Light-grown, homozygous 4-day-old seedlings of each line demonstrated slight but significant root and shoot stunting in comparison to an eGFP amiRNA control (Figure 6b; $p < .05$, *t*-test). However, no significant difference in adult plant height was observed for homozygous plants grown to senescence (Figure 6c; $n = 16$ plants per genotype). This experiment was replicated three times in total, with similar results for each experiment. Final heights varied across plantings due to differences in growth conditions, but in no case was growth inhibition of the *BdGT43B2* amiRNA plants observed relative to control plants.

3.8 | *BdGT43B2* amiRNA plants do not show altered expression of *BdGT43B1* or *BdGT43A2*

Phylogenetic analysis of *Brachypodium distachyon* GT43 members shows that there are eight members in Clade A and two members in Clade B, one of which is *BdGT43B2* (Whitehead et al., 2018).

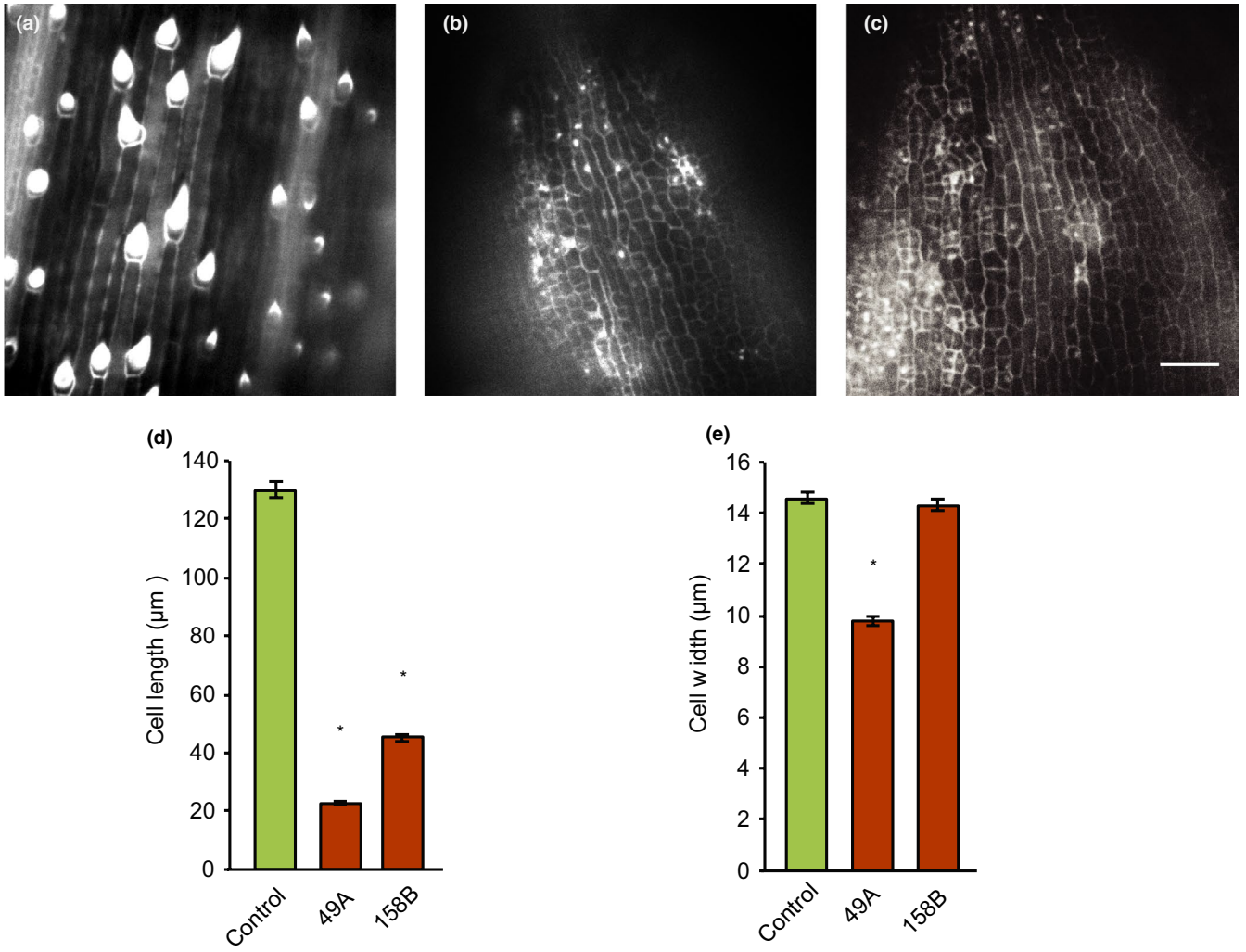

FIGURE 5 Cell dimension analysis of *BdGT43B2* CRISPR lines 49A and 158B in comparison to transgenic control. (a–c) Representative images of light-grown 4 dag cotyledenous leaves stained with 0.1 mg/ml propidium iodide prior to fluorescent imaging using 561 nm laser. (a) eGFP CRISPR Line 81A; (b) *BdGT43B2* CRISPR Line 49A; (c) *BdGT43B2* CRISPR line 158B; (d) Comparison of average cell length in microns; (e) Comparison of average cell width in microns. Scale bar in panel c represents the scale for panels a–c and equals 50 µm. Asterisks in panels d and e show statistical significance at $p < .05$ by Student's *t*-test (2- tailed, type 3) to the transgenic control

To determine whether *BdGT43B1* (*Bradi5g24290*) or *BdGT43A2* (*Bradi5g02350*) exhibit altered expression in *BdGT43B2* amiRNA plants, qRT-PCR experiments were performed. No significant difference was observed in the expression levels of *BdGT43B2* or *BdGT43A2* in *BdGT43B2* amiRNA lines 86A and 12A relative to controls (Figure S2).

3.9 | *BdGT43B2* amiRNA seedlings show minor reduction in xylose content, but no significant reduction in LM11 immunolabeling

To analyze the wall composition of *BdGT43B2* amiRNA plants, AIR was extracted from shoots of 3-day-old *BdGT43B2* amiRNA and eGFP amiRNA control seedlings and hydrolyzed using 2M methanolic HCl, followed by 2M Trifluoroacetic Acid (TFA) incubation. Monosaccharide analysis of hydrolyzed cell walls showed that *BdGT43B2* amiRNA lines 86A and 12A contained 2.3% and 3.3% less xylose than the transgenic control, respectively. These differences were statistically significant ($p < .05$, *t*-test), as were minor increases in rhamnose and galactose. The mean percentage of glucose was 1.61% less in line 86A and 2.35% less in line 12A, although this difference was statistically significant only for the latter. Furthermore, line 12A showed a greater molar percentage of GalA than the transgenic control, whereas line 86A did not (Table 2). Unlike *BdGT43B2* CRISPR mesocotyls, mesocotyls of *BdGT43B2* amiRNA seedlings showed only minor and inconsistent reductions in xylan labeling with LM11 antibody in comparison to the eGFP amiRNA transgenic control (Figure S1).

4 | DISCUSSION

Xylan is a complex and abundant hemicellulose in the primary walls of grasses, which constitute a critically important class of plants

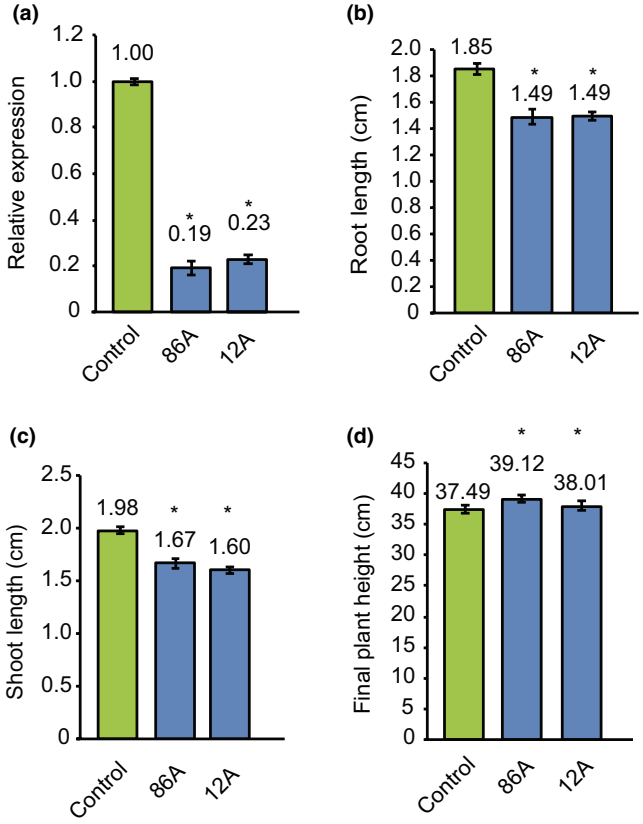

FIGURE 6 Gene expression and associated phenotypes of *BdGT43B2* amiRNA plants. (a) Semi-quantitative reverse-transcription PCR of *BdGT43B2* amiRNA lines 86A and 12A relative to transgenic control. Lines 86A and 12A exhibited 19% and 23% BdGT43B2 gene expression relative to the transgenic control. Three technical replicates were performed per each of three biological replicates (T1 siblings) per transgenic line. The *BdGT43B2* relative expression was significantly different from the control for both amiRNA lines 86A and 12A (Student's *t*-test, unequal variance, $p < .05$). (b) *BdGT43B2* amiRNA light-grown seedling root length. Homozygous T2, T3, and T4 seeds of each amiRNA line and the amiRNA transgenic control construct were germinated on ½ MS + 0% sucrose + 40 µg/ml Hygromycin for four days before measurement. Hygromycin selection was used because although homozygous T2 populations of the *BdGT43B2* amiRNA lines 86A and 12A were isolated, a homozygous T2 population of the eGFP amiRNA transgenic control was not. Data were combined over 6 experimental replicates. Lines 86A and 12A each exhibited a mean that was 80.5% of the seedling root length of the transgenic control mean ($n \geq 184$ per transgenic line). (c) *BdGT43B2* amiRNA light-grown seedling shoot length. Lines 86A and 12A exhibited 84.3% and 80.8% the mean shoot length of the transgenic control, respectively. These differences in root and shoot lengths were significant (Student's *t*-test, unequal variance, asterisks indicate $p < .05$). (d) Final heights of *BdGT43B2* amiRNA T2 homozygous plants, and hygromycin resistant amiRNA transgenic control plants (all initially hygromycin selected as seedlings). No significant difference was observed (Student's *t*-test, unequal variance). $n = 16$ plants per genotype as only a subset of the seedlings germinated on ½ MS + 0% sucrose + 40 µg/ml Hygromycin were transferred to soil. Error bars represent standard error

for the production of food and bioenergy. To determine the biological role in growth and development of the putative xylan synthase gene *BdGT43B2*, we generated and characterized CRISPR/Cas9 functional knockout and amiRNA knockdown mutants. Plants homozygous for frameshift mutations in *BdGT43B2* exhibited seedling stunting and died within 2 weeks of germination (Figures 1 and 2). *BdGT43B2* CRISPR knockout mutants exhibited greatly reduced labeling of the xylan-specific LM11 antibody in mesocotyl sections, whereas S4B staining for cellulose was slightly increased (Figure 3). This increase in S4B staining might be due to an increased accessibility to the cellulose in the localized absence of xylan, or to increased cellulose abundance, which might inhibit cell expansion. The morphology of sections taken the same distance from the connection between the etiolated shoot and the base of the seed differed between *BdGT43B2* CRISPR and transgenic control lines, with the mesocotyl, and internal vascular cylinder appearing smaller in diameter in the *BdGT43B2* CRISPR lines. To address whether this morphological difference is due to decreased growth versus a developmental delay, antibodies to detect germin accumulation during cereal grain germination of the *BdGT43B2* CRISPR versus controls could be used (Lane, Dunwell, Ray, Schmitt, & Cuming, 1993). As a glycoprotein whose synthesis is associated with the onset of growth in germinating wheat embryos, monitoring the accumulation of germin in the *BdGT43B2* mutants versus controls might provide data to support or refute a developmental delay in these seedlings.

Despite *BdGT43B2* knockout, xylan was still detected, albeit at a reduced level, in seedling cell wall material analyzed by PACE. Perhaps the normal level of *BdGT43B1* (*Bradi5g24290*) expression observed in the *BdGT43B2* mutants allows enough xylan production to be detectable by PACE (Figure 4). However, either the amount or substitution pattern of xylan that is produced when only BdGT43B1 is present as part of the XSC, rather than both BdGT43B1 and BdGT43B2, was not sufficient for *BdGT43B2* CRISPR knockout seedling survival.

The question of why knockout of BdGT43B2 led to a lethal phenotype where plants were unable to develop beyond seedling stage, but BdGT43B2 knockdown was not lethal, deserves consideration. It is possible that compensatory expression of other GT43 members is triggered in BdGT43B2 knockdown plants, providing functional redundancy later in development that allows plants to grow to adulthood, but differential expression of Bradi5g24290 or Bradi5g02350, other genes that encode putative xylan synthases (Whitehead et al., 2018), was not observed (Figure S2). *Bradi5g24290* was selected for examination due to publication (Whitehead et al., 2018) describing a non-synonymous SNP mutant having altered cell wall composition resulting in increased saccharification of straw. *Bradi5g02350* was selected based on strong expression in leaves throughout development (particularly in leaves 10 dag), first internodes, and roots 10 dag (*Brachypodium distachyon* eFP Browser at http://bar.utoronto.ca; Sibout et al., 2017; Winter

TABLE 1 Sequence of *BdGT43B2* Fr/Fr regenerated plant lines

Line	Allele 1 Sequence Surrounding (TT) DSB site	Mutation	Allele 2 Sequence Surrounding (TT) DSB site	Mutation
WT	CTCCCTC**TT**CCTCGGGTTCC	0	CTCCCTC**TT**CCTCGGGTTCC	0
114A	CTCCCTC**T**CCTCGGGTTCC	1 T DEL	CTCCCTC**T**CCTCGGGTTCC	1 T DEL
158A	CTCCCTC**TtT**CCTCGGGTTCC	1 T INS	CTCCCTC**TtT**CCTCGGGTTCC	1 T INS
188A1	CTCCCTC**TtT**CCTCGGGTTCC	1 T INS	CTCCCTC**TcT**CCTCGGGTTCC	1 C INS
80A	CTCCCTC**TaT**CCTCGGGTTCC	1 A INS	CTCCCTC**TaT**CCTCGGGTTCC	1 A INS
83A	CTCCCTC**TtT**CCTCGGGTTCC	1 T INS	CTCCCTC**T**CCTCGGGTTCC	1 T DEL

Note: The WT control sequence is shown in the top row for comparison. The two Ts that surround the double-stranded break site (DSB) are shown in boldface. On the coding strand sequence (shown), the only nucleotides deleted across these five Fr/Fr lines was one of the two Ts surrounding the double-stranded base site. Inserted nucleotides are shown in lower case. PCR products were generated using the pCTA2525 and pCTA2526 primers, and these products were sequenced in both directions using these primers as sequencing primers.

TABLE 2 Monosaccharide analysis of *BdGT43B2* amiRNA plants versus transgenic control

Transgenic line	Fuc	Rha	Ara	Gal	Glc	Xyl	GalA	GlcA
Control	0.25 ± 0.12	1.30 ± 0.06	17.05 ± 1.51	7.55 ± 0.47	24.47 ± 2.17	42.49 ± 1.44	6.27 ± 0.84	0.62 ± 0.15
86A	0.24 ± 0.14	**1.48 ± 0.08**	17.27 ± 0.51	**7.93 ± 0.08**	26.08 ± 1.43	**40.18 ± 1.34**	6.28 ± 0.22	0.54 ± 0.07
12A	0.32 ± 0.21	**1.56 ± 0.17**	16.11 ± 1.53	**8.08 ± 0.18**	**26.82 ± 1.12**	**39.19 ± 0.75**	**7.32 ± 0.31**	0.60 ± 0.14

Note: Sugar composition from 3-day-old etiolated shoots of the transgenic control (eGFP amiRNA), *BdGT43B2* amiRNA Line 86A, and *BdGT43B2* amiRNA Line 12A genotypes. Sugar amounts are presented as mean percentages, with standard deviation shown below (n = 3 technical replicates per each of three biological replicates). Bold values indicate glycosyl residue compositions that are significantly different (Student's t-test, $p < .05$) compared to the transgenic control.

et al., 2007). As mentioned, no differential expression was measured for *Bradi5g24290* or *Bradi5g02350* in the 27 dag leaf tissue that was used to measure reduced expression of *BdGT43B2*. The simplest explanation for *BdGT43B2* amiRNA mediated gene knockdown not being lethal, unlike lethality observed in the *BdGT43B2* CRISPR Fr/Fr seedlings, is that the approximately 20% *BdGT43B2* expression remaining in the amiRNA lines allowed sufficient production of the IRX14 scaffolding protein, such that the amount of xylan deposited in the primary cell wall was only slightly diminished (~2%–3% less xylose detected by monosaccharide analysis). The *BdGT43B2* amiRNA immunolabeling experiments showed significant reduction of LM11 binding (31% and 5% of the control level of fluorescence for lines 86A and 12A, respectively). Given that the monosaccharide compositional analysis (Table 2) detected only a 2%–3% decrease in xylose extracted from the seedling cell walls, this suggests that the LM11 binding epitope on xylan was particularly affected by *BdGT43B2* expression reduction. This interpretation is substantiated by the PACE data of the *BdGT43B2* amiRNA lines, which showed minor to insignificant reduction of xylan fragments in comparison to the transgenic control (Figure S3). Taking the knockout and knockdown data together, we conclude that the BdGT43B2 protein might be preferentially used in XSCs during seed germination and seedling growth, and its lack may be the cause of the quantified reduction in cell elongation (Figure 5). Given the function of xylan in secondary wall formation in eudicots and monocots (Faik, 2010), we considered the possibility that premature death of the knockout seedlings might occur due to collapsed vasculature, but obvious xylem vessel collapse was not observed in seedling stem cross sections. Attempts to keep knockout seedlings alive by growing them in high humidity to compensate for deficient transpirational cooling were unsuccessful. The fact that *BdGT43B2* amiRNA seedlings exhibited only minor reduction in xylan binding to the LM11 antibody is consistent with the ~ 2%–3% xylose reduction observed via monosaccharide analysis. Perhaps low *BdGT43B2* gene expression is sufficient to produce enough functional XSCs such that growth is only slightly affected at the seedling stage (Figure 6), and no height deficiency was observed in adult plants.

Although obtaining enough tissue to perform monosaccharide analysis on the *BdGT43B2* CRISPR knockouts was not possible, *BdGT43B2* amiRNA seedlings exhibited moderate stunting (Figure 6), and monosaccharide analysis showed a xylose reduction in the *BdGT43B2* amiRNA lines 86A and 12A of 2.3% and 3.3%, respectively. Xylose also exists in xyloglucan in the cell walls of grasses, but xyloglucan represents only 1%–5% dry weight of the grass primary wall, and is present in even lower amounts in the secondary cell wall (Vogel, 2008). Therefore, we conclude that the decrease in xylose content observed in *BdGT43B2* amiRNA seedlings is more likely to result from a reduction in xylan content than from a reduction in xyloglucan.

Despite primary wall xylan being nonessential in *Arabidopsis thaliana* (Mortimer et al., 2015), it has been noted that knockout of both IRX14/14L and IRX9/9L leads to extreme stunting of seedlings, and a lack of inflorescence production after 6 weeks (Wu et al., 2010), for reasons yet to be elucidated. Therefore, there is some a priori evidence that makes it reasonable to presume that similar defects in

growth and development may be induced by xylan depletion in the primary cell walls of grasses.

In conclusion, we demonstrated that *BdGT43B2* is an essential gene in *Brachypodium distachyon* and that BdGT43B2 likely functions in the synthesis of a type of xylan that is important for seedling survival. As researchers engineer xylan content in grasses to generate higher-yielding and/or more easily digestible biomass, consideration of the complexity of xylan synthesis, substitution, and function at specific developmental phases will be key to deciphering this enigmatic cell wall polymer.

ACKNOWLEDGMENTS

The authors would like to thank Benjamin Ratchford and Jonathan Puglisi for their assistance in cell length and width measurements used to obtain data for Figure 5. This work was supported as part of The Center for Lignocellulose Structure and Formation, an Energy Frontier Research Center funded by the U.S. Department of Energy, Office of Science, Basic Energy Sciences under Award # DE-SC0001090.

CONFLICT OF INTEREST

The authors declare no conflict of interest.

AUTHOR CONTRIBUTIONS

DLP, TT, PD and CTA designed the research; DLP and TT performed experiments; DLP, TT, PD and CTA analyzed data; DLP, TT, PD and CTA wrote the paper.

ORCID

Deborah L. Petrik https://orcid.org/0000-0003-3711-6480
Theodora Tryfona https://orcid.org/0000-0002-1618-3521
Paul Dupree https://orcid.org/0000-0001-9270-6286
Charles T. Anderson https://orcid.org/0000-0001-7481-3571

REFERENCES

Anderson, C. T., Carroll, A., Akhmetova, L., & Somerville, C. R. (2010). Real time imaging of cellulose reorientation during cell wall expansion in Arabidopsis roots. *Plant Physiology*, *152*(2), 787–796. https://doi.org/10.1104/pp.109.150128

Bragg, J. N., Anderton, A., Nieu, R., & Vogel, J. P. (2015). *Brachypodium distachyon*. In *Agrobacterium Protocols* (pp. 17–33). New York, NY: Springer.

Brown, D. M., Goubet, F., Wong, V. W., Goodacre, R., Stephens, E., Dupree, P., & Turner, S. R. (2007). Comparison of five xylan synthesis mutants reveals new insight into the mechanisms of xylan synthesis. *Plant Journal*, *52*(6), 1154–1168. https://doi.org/10.1111/j.1365-313X.2007.03307.x

Brown, D. M., Zhang, Z., Stephens, E., Dupree, P., & Turner, S. R. (2009). Characterization of IRX10 and IRX10-like reveals an essential role in glucuronoxylan biosynthesis in Arabidopsis. *The Plant Journal*, *57*(4), 732–746.

Busse-Wicher, M., Gomes, T. C., Tryfona, T., Nikolovski, N., Stott, K., Grantham, N. J., … Dupree, P. (2014). The pattern of xylan acetylation suggests xylan may interact with cellulose microfibrils as a twofold helical screw in the secondary plant cell wall of Arabidopsis thaliana. *The Plant Journal*, *79*(3), 492–506.

Chen, X., Vega-Sánchez, M. E., Verhertbruggen, Y., Chiniquy, D., Canlas, P. E., Fagerström, A., … Ronald, P. C. (2013). Inactivation of OsIRX10 leads to decreased xylan content in rice culm cell walls and improved biomass saccharification. *Molecular Plant*, *6*(2), 570–573.

Chiniquy, D., Varanasi, P., Oh, T., Harholt, J., Katnelson, J., & Singh, S., … Ronald, P. C. (2013). Three novel rice genes closely related to the Arabidopsis IRX9, IRX9L, and IRX14 genes and their roles in Xylan biosynthesis. *Frontiers in Plant Science*, *4*, 83.

Cosgrove, D. J. (2018). Nanoscale structure, mechanics and growth of epidermal cell walls. *Current Opinion in Plant Biology*, *46*, 77–86. https://doi.org/10.1016/j.pbi.2018.07.016

Faik, A. (2010). Xylan biosynthesis: News from the grass. *Plant Physiology*, *153*(2), 396–402. https://doi.org/10.1104/pp.110.154237

Freeman, J., Lovegrove, A., Wilkinson, M. D., Saulnier, L., Shewry, P. R., & Mitchell, R. A. C. (2016). Effect of suppraession of arabinoxylan synthetic genes in wheat endosperm on chain length of arabinoxylan and extract viscosity. *Plant Biotechnology Journal*, *14*(1), 109–116. https://doi.org/10.1111/pbi.12361

Gilbert, H. J., Hazlewood, G. P., Laurie, J. I., Orpin, C. G., & Xue, G. P. (1992). Homologous catalytic domains in a rumen fungal xylanase: Evidence for gene duplication and prokaryotic origin. *Molecular Microbiology*, *6*(15), 2065–2072. https://doi.org/10.1111/j.1365-2958.1992.tb01379.x

Goubet, F., Barton, C. J., Mortimer, J. C., Yu, X., Zhang, Z., Miles, G. P., … Dupree, P. (2009). Cell wall glucomannan in Arabidopsis is synthesised by CSLA glycosyltransferases, and influences the progression of embryogenesis. *The Plant Journal*, *60*(3), 527–538. https://doi.org/10.1111/j.1365-313X.2009.03977.x

Goubet, F., Jackson, P., Deery, M. J., & Dupree, P. (2002). Polysaccharide analysis using carbohydrate gel electrophoresis: A method to study plant cell wall polysaccharides and polysaccharide hydrolases. *Analytical Biochemistry*, *300*(1), 53–68. https://doi.org/10.1006/abio.2001.5444

Grantham, N. J., Wurman-Rodrich, J., Terrett, O. M., Lyczakowski, J. J., Stott, K., Iuga, D., … Dupree, P. (2017). An even pattern of xylan substitution is critical for interaction with cellulose in plant cell walls. *Nature Plants*, *3*(11), 859. https://doi.org/10.1038/s41477-017-0030-8

Jensen, J. K., Johnson, N. R., & Wilkerson, C. G. (2014). Arabidopsis thaliana IRX 10 and two related proteins from psyllium and Physcomitrella patens are xylan xylosyltransferases. *The Plant Journal*, *80*(2), 207–215.

Jiang, N., Wiemels, R. E., Soya, A., Whitley, R., Held, M., & Faik, A. (2016). Composition, assembly, and trafficking of a wheat xylan synthase complex. *Plant Physiology*, *170*(4), 1999–2023. https://doi.org/10.1104/pp.15.01777

Keppler, B. D., & Showalter, A. M. (2010). IRX14 and IRX14-LIKE, two glycosyl transferases involved in glucuronoxylan biosynthesis and drought tolerance in Arabidopsis. *Molecular Plant*, *3*(5), 834–841. https://doi.org/10.1093/mp/ssq028

Köhnke, T., Östlund, Å., & Brelid, H. (2011). Adsorption of arabinoxylan on cellulosic surfaces: Influence of degree of substitution and substitution pattern on adsorption characteristics. *Biomacromolecules*, *12*(7), 2633–2641. https://doi.org/10.1021/bm200437m

Lane, B. G., Dunwell, J. M., Ray, J. A., Schmitt, M. R., & Cuming, A. C. (1993). Germin, a protein marker of early plant development, is an oxalate oxidase. *Journal of Biological Chemistry*, *268*(17), 12239–12242.

Lee, C., O'Neill, M. A., Tsumuraya, Y., Darvill, A. G., & Ye, Z. H. (2007). The irregular xylem9 mutant is deficient in xylan xylosyltransferase

activity. *Plant and Cell Physiology*, *48*(11), 1624–1634. https://doi.org/10.1093/pcp/pcm135

Lee, C., Teng, Q., Huang, W., Zhong, R., & Ye, Z.-H. (2010). The Arabidopsis family GT43 glycosyltransferases form two functionally nonredundant groups essential for the elongation of glucuronoxylan backbone. *Plant Physiology*, *153*, 526–541. https://doi.org/10.1104/pp.110.155309

Lovegrove, A., Wilkinson, M. D., Freeman, J., Pellny, T. K., Tosi, P., Saulnier, L., … Mitchell, R. A. C. (2013). RNA interference suppression of genes in glycosyl transferase families 43 and 47 in wheat starchy endosperm causes large decreases in arabinoxylan content. *Plant Physiology*, *163*(1), 95–107.

Margolles-Clark, E., Tenkanen, M., Nakari-Setälä, T. I. I. N. A., & Penttilä, M. (1996). Cloning of genes encoding alpha-L-arabinofuranosidase and beta-xylosidase from Trichoderma reesei by expression in Saccharomyces cerevisiae. *Applied and Environment Microbiology*, *62*(10), 3840–3846. https://doi.org/10.1128/AEM.62.10.3840-3846.1996

Mortimer, J. C. (2017). Structural analysis of cell wall polysaccharides using PACE. *Methods in Molecular Biology*, *1544*, 223-231.

Mortimer, J. C., Faria-Blanc, N., Yu, X., Tryfona, T., Sorieul, M., Ng, Y. Z., … Dupree, P. (2015). An unusual xylan in Arabidopsis primary cell walls is synthesised by GUX3, IRX9L, IRX10L and IRX14. *The Plant Journal*, *83*(3), 413–426.

Raju, M. V. S., & Steeves, T. A. (1998). Growth, anatomy and morphology of the mesocotyl and the growth of appendages of the wild oat (*Avena fatua* L.) seedling. *Journal of Plant Research*, *111*(1), 73–85. https://doi.org/10.1007/BF02507152

Rancour, D., Marita, J., & Hatfield, R. D. (2012). Cell wall composition throughout development for the model grass *Brachypodium distachyon*. *Frontiers in Plant Science*, *3*, 266. https://doi.org/10.3389/fpls.2012.00266

Ren, Y., Hansen, S. F., Ebert, B., Lau, J., & Scheller, H. V. (2014). Site-directed mutagenesis of IRX9, IRX9L and IRX14 proteins involved in xylan biosynthesis: Glycosyltransferase activity is not required for IRX9 function in Arabidopsis. *PLoS ONE*, *9*(8), e105014. https://doi.org/10.1371/journal.pone.0105014

Rennie, E. A., & Scheller, H. V. (2014). Xylan biosynthesis. *Current Opinion in Biotechnology*, *26*, 100–107. https://doi.org/10.1016/j.copbio.2013.11.013

Rogowski, A., Baslé, A., Farinas, C. S., Solovyova, A., Mortimer, J. C., Dupree, P., … Bolam, D. N. (2014). Evidence that GH115 α-glucuronidase activity, which is required to degrade plant biomass, is dependent on conformational flexibility. *Journal of Biological Chemistry*, *289*(1), 53–64. https://doi.org/10.1074/jbc.M113.525295

Ruprecht, C., Bartetzko, M. P., Senf, D., Dallabernadina, P., Boos, I., Andersen, M. C. F., … Pfrengle, F. (2017). A synthetic glycan microarray enables epitope mapping of plant cell wall glycan-directed antibodies. *Plant Physiology*, *175*(3), 1094–1104. https://doi.org/10.1104/pp.17.00737

Saka, S., & Bae, H. J. (2016). Secondary xylem for bioconversion. In K. Yoon soo, F. Ryo & P. S. Adya (Eds.), *Secondary xylem biology: origins, functions, and applications* (pp. 213–231). Academic Press. https://doi.org/10.1016/B978-0-12-802185-9.00011-5

Sibout, R., Proost, S., Hansen, B. O., Vaid, N., Giorgi, F. M., Ho-Yue-Kuang, S., … Soulhat, C. (2017). Expression atlas and comparative coexpression network analyses reveal important genes involved in the formation of lignified cell wall in Brachypodium distachyon. *New Phytologist*, *215*, 1009–1025.

Simmons, T. J., Mortimer, J. C., Bernardinelli, O. D., Pöppler, A.-C., Brown, S. P., deAzevedo, E. R., … Dupree, P. (2016). Folding of xylan onto cellulose fibrils in plant cell walls revealed by solid-state NMR. *Nature Communications*, *7*, 13902. https://doi.org/10.1038/ncomms13902

Tryfona, T., Sorieul, M., Feijao, C., Stott, K., Rubtsov, D. V., Anders, N., & Dupree, P. (2019). Development of an oligosaccharide library to characterise the structural variation in glucurono-arabinoxylan in the cell walls of vegetative tissues in grasses. *Biotechnology for Biofuels*, *12*(1), 109. https://doi.org/10.1186/s13068-019-1451-6

Urbanowicz, B. R., Peña, M. J., Moniz, H. A., Moremen, K. W., & York, W. S. (2014). Two arabidopsis proteins synthesize acetylated xylan in vitro. *The Plant Journal*, *80*(2), 197–206.

Vogel, J. (2008). Unique aspects of the grass cell wall. *Current Opinion in Plant Biology*, *11*(3), 301–307. https://doi.org/10.1016/j.pbi.2008.03.002

Vogel, J., Garvin, D., Mockler, T., Schmutz, J., Rokhsar, D., Bevan, M., … Tice, H. (2010). Genome sequencing and analysis of the model grass *Brachypodium distachyon*. *Nature*, *463*(7282), 763–768.

Vogel, J., & Hill, T. (2008). High-efficiency Agrobacterium-mediated transformation of *Brachypodium distachyon* inbred line Bd21-3. *Plant Cell Reports*, *27*(3), 471–478. https://doi.org/10.1007/s00299-007-0472-y

Wende, G., & Fry, S. C. (1997). 2-O-β-d-xylopyranosyl-(5-O-feruloyl)-l-arabinose, a widespread component of grass cell walls. *Phytochemistry*, *44*(6), 1019–1030. https://doi.org/10.1016/S0031-9422(96)00649-8

Whitehead, C., Ostos Garrido, F. J., Reymond, M., Simister, R., Distelfeld, A., Atienza, S. G., … McQueen-Mason, S. J. (2018). A glycosyl transferase family 43 protein involved in xylan biosynthesis is associated with straw digestibility in Brachypodium distachyon. *New Phytologist*, *218*(3), 974–985.

Winter, D., Vinegar, B., Nahal, H., Ammar, R., Wilson, G. V., & Provart, N. J. (2007). An "Electronic Fluorescent Pictograph" browser for exploring and analyzing large-scale biological data sets. *PLoS ONE*, *2*, e718. https://doi.org/10.1371/journal.pone.0000718

Wu, A. M., Hörnblad, E., Voxeur, A., Gerber, L., Rihouey, C., Lerouge, P., & Marchant, A. (2010). Analysis of the Arabidopsis IRX9/IRX9-L and IRX14/IRX14-L pairs of glycosyltransferase genes reveals critical contributions to biosynthesis of the hemicellulose glucuronoxylan. *Plant Physiology*, *153*(2), 542–554.

Xiao, C., Somerville, C., & Anderson, C. T. (2014). POLYGALACTURONASE INVOLVED IN EXPANSION1 functions in cell elongation and flower development in Arabidopsis. *Plant Cell*, *26*(3), 1018–1035.

Xie, K., Minkenberg, B., & Yang, Y. (2014). Targeted gene mutation in rice using a CRISPR-Cas9 system. *Bio Protoc*, *4*, e1225. https://doi.org/10.21769/BioProtoc.1225

Xie, K., Minkenberg, B., & Yang, Y. (2015). Boosting CRISPR/Cas9 multiplex editing capability with the endogenous tRNA-processing system. *Proceedings of the National Academy of Sciences*, *112*(11), 3570–3575. https://doi.org/10.1073/pnas.1420294112

Xie, K., Zhang, J., & Yang, Y. (2014). Genome-wide prediction of highly specific guide RNA spacers for CRISPR–Cas9-mediated genome editing in model plants and major crops. *Molecular Plant*, *7*(5), 923–926. https://doi.org/10.1093/mp/ssu009

Zeng, W., Chatterjee, M., & Faik, A. (2008). UDP-xylose-stimulated glucuronyltransferase activity in wheat microsomal membranes: characterization and role in glucurono (arabino) xylan biosynthesis. *Plant physiology*, *147*(1), 78–91.

Zeng, W., Jiang, N., Nadella, R., Killen, T. L., Nadella, V., & Faik, A. (2010). A glucurono (arabino) xylan synthase complex from wheat contains members of the GT43, GT47, and GT75 families and functions cooperatively. *Plant Physiology*, *154*(1), 78–97. https://doi.org/10.1104/pp.110.159749

Zeng, W., Lampugnani, E. R., Picard, K. L., Song, L., Wu, A.-M., Farion, I. M., … Bacic, A. (2016). Asparagus IRX9, IRX10, and IRX14A are components of an active xylan backbone synthase complex that forms

in the Golgi apparatus. *Plant Physiology*, *171*(1), 93–109. https://doi.org/10.1104/pp.15.01919

SUPPORTING INFORMATION

Additional supporting information may be found online in the Supporting Information section.

How to cite this article: Petrik DL, Tryfona T, Dupree P, Anderson CT. BdGT43B2 functions in xylan biosynthesis and is essential for seedling survival in *Brachypodium distachyon*. *Plant Direct*. 2020;4:1–16. https://doi.org/10.1002/pld3.216